



HAL
open science

Solution of the radiative transfer equation in an absorbing and scattering Nd:YAG laser-induced plume

David Lacroix, G. Jeandel, C. Boudot

► **To cite this version:**

David Lacroix, G. Jeandel, C. Boudot. Solution of the radiative transfer equation in an absorbing and scattering Nd:YAG laser-induced plume. *Journal of Applied Physics*, 1998, 84 (5), pp.2443 - 2449. 10.1063/1.368405 . hal-01887304

HAL Id: hal-01887304

<https://hal.science/hal-01887304>

Submitted on 3 Oct 2018

HAL is a multi-disciplinary open access archive for the deposit and dissemination of scientific research documents, whether they are published or not. The documents may come from teaching and research institutions in France or abroad, or from public or private research centers.

L'archive ouverte pluridisciplinaire **HAL**, est destinée au dépôt et à la diffusion de documents scientifiques de niveau recherche, publiés ou non, émanant des établissements d'enseignement et de recherche français ou étrangers, des laboratoires publics ou privés.

Solution of the radiative transfer equation in an absorbing and scattering Nd:YAG laser-induced plume

D. Lacroix, G. Jeandel, and C. Boudot

Citation: *J. Appl. Phys.* **84**, 2443 (1998); doi: 10.1063/1.368405

View online: <http://dx.doi.org/10.1063/1.368405>

View Table of Contents: <http://jap.aip.org/resource/1/JAPIAU/v84/i5>

Published by the [American Institute of Physics](http://www.aip.org).

Related Articles

Light down-conversion with over 100% external quantum efficiency in bulk germanium

Appl. Phys. Lett. **101**, 081111 (2012)

Nanoscale thermal radiation between two gold surfaces

Appl. Phys. Lett. **100**, 233114 (2012)

Emissivity measurements with an atomic force microscope

J. Appl. Phys. **111**, 063110 (2012)

Asymptotic expressions describing radiative heat transfer between polar materials from the far-field regime to the nanoscale regime

J. Appl. Phys. **111**, 014311 (2012)

Penetration depth in near-field radiative heat transfer between metamaterials

Appl. Phys. Lett. **99**, 143107 (2011)

Additional information on J. Appl. Phys.

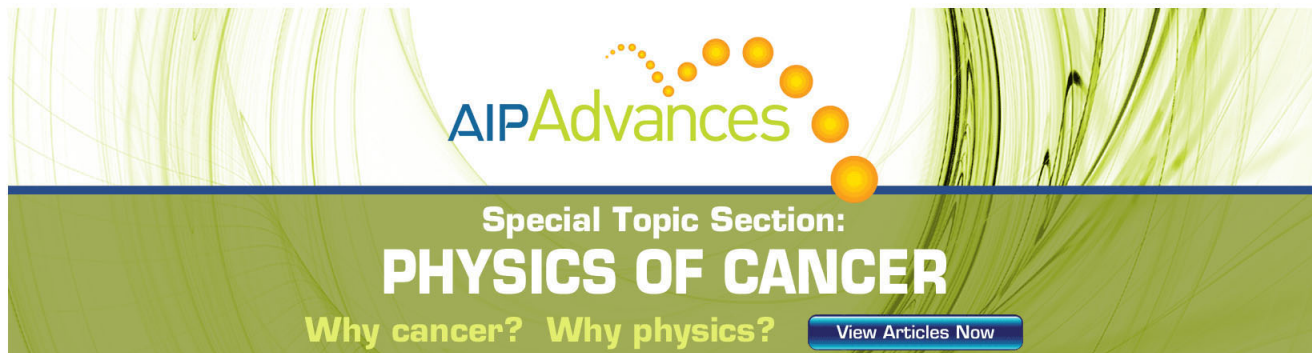
Journal Homepage: <http://jap.aip.org/>

Journal Information: http://jap.aip.org/about/about_the_journal

Top downloads: http://jap.aip.org/features/most_downloaded

Information for Authors: <http://jap.aip.org/authors>

ADVERTISEMENT



AIP Advances

Special Topic Section:
PHYSICS OF CANCER

Why cancer? Why physics? [View Articles Now](#)

Solution of the radiative transfer equation in an absorbing and scattering Nd:YAG laser-induced plume

D. Lacroix^{a)} and G. Jeandel

LEMTA, Faculté des Sciences Henri Poincaré, Nancy I, B. P. 239,
54506 Vandoeuvre-lès-Nancy cedex, France

C. Boudot

FRAMATOME, Z. I. et portuaire sud, B. P. 13, 71380 St. Marcel, France

(Received 26 November 1997; accepted for publication 1 June 1998)

We analyze the scattering effect in a laser-induced plasma plume in the case of a Nd:YAG laser welding process using a discrete ordinate scheme and the radiative transfer equation. The optical properties of plume vapors from stainless steel are analyzed at various temperatures as different parameters are varied (laser wavelength, plasma pressure and composition, type of shielding gas). The scattering coefficients and the phase function due to the presence of small particles in the plume are calculated using the Mie theory for different particle diameters and several densities of particles in the medium. With our model we estimate the temperature in the plasma plume. © 1998 American Institute of Physics. [S0021-8979(98)04617-9]

I. INTRODUCTION

Numerical analysis of welding process phenomena has developed considerably over recent years, especially as regards characterization of the laser-matter interaction through the keyhole. There are several good models for describing laser beam absorption inside the keyhole. The most recent¹⁻⁴ are complex, and include many parameters such as the motion of molten metal, keyhole geometry, and the energy distribution inside a laser beam. These models are useful for predicting the weld seam profile, but there is no simple way of estimating the effect of the plume on heat transfer.

Few studies deal with laser-plasma interactions above the keyhole. Beck *et al.*⁵ study the defocusing effect due to the formation of plasma in CO₂ welding and explain that the focus of a CO₂ laser beam is sharply degraded by refraction and absorption inside the plasma plume. They show the dependence of the complex optical index on temperature and on the type of shielding gas used during welding, and say that one good way to enhance the stability of the process is to use a 3:1 mixture of helium and argon. But, this study does not consider scattering due to the particles that, as Matsunawa and Ohnawa⁶ showed, exist inside the plume. According to these authors, the scattering of the laser beam cannot be neglected.

Poueyo-Verwaerde *et al.*⁷ explain that the plume absorbs a significant amount of the laser energy in CO₂ welding. They prove that the plasma plume is less absorbent at low pressures, and the resulting weld seam does not exhibit the classical "nail-head" shape, but is thin and has parallel edges. Dumord⁸ also assumes that the plume has a seam-widening effect. She studied the heat transfer in Nd:YAG welding, where the plasma plume is not highly absorbent, and modeled the "nail-head" profile with two components: the keyhole and a spherical heat source due to the scattering

of the laser beam at the metal surface. This model is an improvement on a point-and-line source model. Finally, the presence of small particles inside the plasma plume is also assumed by Gouveia *et al.*⁹ in a paper dealing with CO₂ welding of copper. These authors assume that droplets inside the plume do not vaporize instantaneously but remain molten, due to an increase of the internal pressure caused by surface tension. In this case, particles of several nanometers would exist in the plume and take part in thermal exchanges.

In the present article we introduce a model describing the interactions between a focused laser beam and the plasma plume. The model is based on the solution of the radiative transfer equation in a semitransparent medium. In the first section of the article, we give some details about the classical relations used to determine the absorption coefficient of the plasma plume. We calculate the complex optical index of refraction using electron, neutral, and ionic densities of the medium, at different temperatures and for three different pressures: 10², 10⁵ and 3 × 10⁵ Pa.

In the second section of the article, we describe the scattering of light in a semitransparent medium. We apply Mie's theory to calculate the phase functions, scattering coefficient, and absorption coefficient of a spherical particle at the Nd:YAG laser wavelength ($\lambda = 1.06 \mu\text{m}$).

In the last section, we present the discrete ordinate scheme and give some details concerning the numerical treatment, and then discuss the results of the simulations.

II. PLASMA PROPERTIES

A. Density calculations

The theoretical density of a plasma can be computed numerically. We have developed a model, which uses the following four equations and conditions,^{10,11}

- (i) the Saha equation,
- (ii) mass conservation,

^{a)}Electronic mail: dlacroix@lemta.sciences.u-nancy.fr

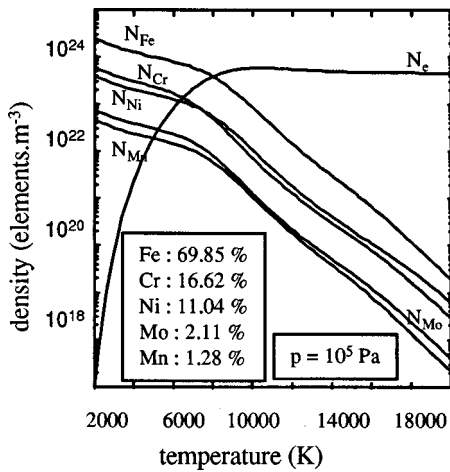


FIG. 1. Stainless steel plasma densities vs temperature.

- (iii) electric neutrality, and
- (iv) the ideal gas equation.

The Saha equation, giving the density ratio between two successive ionization states for a given element, can be written as follows:

$$\frac{N_{i,a}N_e}{N_{i-1,a}} = 2 \frac{Z_{i,a}(T)}{Z_{i-1,a}(T)} \frac{(2\pi mkT)^{3/2}}{h^3} \exp\left[\frac{-(E_\infty^{i-1} - \Delta E_\infty^{i-1})}{kT}\right], \tag{1}$$

in which $N_{i,a}$ is the ionic density, $Z_{i,a}(T)$ the partition function of the element ‘‘a’’ in the ionization state ‘‘i,’’ N_e the electron density, and E_∞^{i-1} the ionization potential of the state ‘‘i-1’’ with respect to state ‘‘i.’’ Details concerning the calculation of $Z_{i,a}(T)$, $N_{i,a}$, and N_e are given in a previous article.¹¹ The densities of each component of a stainless steel plasma are presented in Figs. 1 and 2 for a pressure of 10^5 Pa. In our calculations, we consider that the plasma plume is made of iron, chromium, nickel, molybdenum, and manganese (Fe 69.85%, Cr 16.62%, Ni 11.04%, Mo 2.11%, Mn 1.28%). Electron microscopy measurements of the plasma plume particle composition show that we are close to these values, and the resulting calculated electron density is in good agreement with previous spectroscopic measurements.

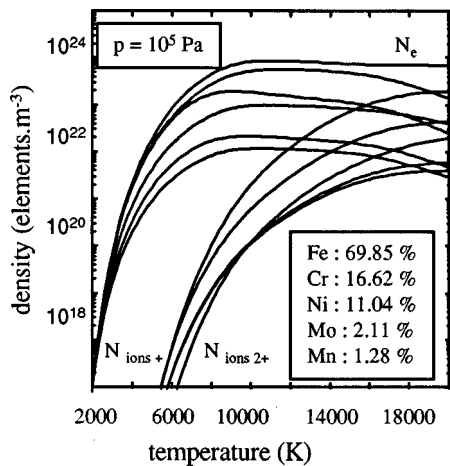


FIG. 2. Stainless steel plasma densities vs temperature.

B. Absorption calculation

The absorption coefficient of the plume is determined by the complex optical index \hat{n} , which depends on the laser frequency ω , the electron collision frequency ω_e , and the plasma frequency ω_p as

$$\hat{n}^2 = 1 - \frac{\omega_p^2}{\omega(\omega - i\omega_e)}, \tag{2}$$

in which

$$\omega = \frac{2\pi c}{\lambda}, \tag{3}$$

and

$$\omega_p^2 = \frac{e^2 N_e}{\epsilon_0 m_e}. \tag{4}$$

The electron collision frequency is the sum of the electron-neutral and electron-ion collision frequencies. We calculate them for each component of the plasma:

$$\omega_e = \sum_{s:\text{species}} \left(\omega_{e-a,s} + \sum_{z:\text{ionization state}} \omega_{e-iz,s} \right). \tag{5}$$

According to Tannenbaum¹² and Mitchener and Kruger,¹³ the collision frequencies between atom and electron and between ion and electron can be written as

$$\omega_{e-a,s} = \frac{8(2\pi)^{3/2}}{3\sqrt{m_e}} (kT_e)^{1/2} N_{a,s} D_{\sigma,s}^2, \tag{6}$$

$$\omega_{e-iz,s} = \frac{z^2 e^4 N_{iz,s}}{3\epsilon_0^2 \sqrt{m_e} (2\pi kT)^{3/2}} \ln(\Lambda), \tag{7}$$

where $N_{a,s}$ is the density of the element s in the neutral state, $D_{\sigma,s}$ a collisional parameter, which is $D_{\sigma,s} = 1.26 \times 10^{-10}$ m for iron, $\ln(\Lambda)$ is the Coulomb logarithm, and $N_{iz,s}$ is the density of the element s in the ionization state z .

From the complex index of refraction, we can derive the refractive index n and the absorption coefficient α of the plasma plume by

$$n = \text{Re}(\hat{n}), \tag{8}$$

and

$$\alpha = \frac{4\pi \text{Im}(\hat{n})}{\lambda}. \tag{9}$$

Figures 3 and 4 present the variation of n and α as a function of temperature for the three pressures mentioned above. We see that the wavelength has a major effect on the absorption coefficient. At the CO_2 wavelength, α is a hundred times greater than at the Nd:YAG wavelength. Absorption in the plasma plume is due to inverse bremsstrahlung. Electron-ion collisions are preponderant in the variation of the absorption. Maximum values of α are reached around 9000 K. The absorption varies strongly depending on the pressure of the medium. At low pressures (10^2 Pa), the plume is no longer absorbent.

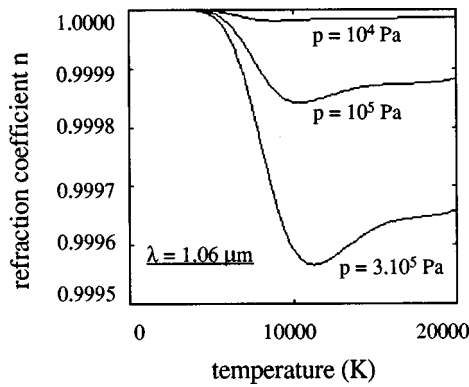


FIG. 3. Refraction index vs temperature for different pressures.

In our further calculations we consider a Nd:YAG laser-induced plume at atmospheric pressure. In this case, the refractive index is almost equal to unity, and $\alpha = 3 \text{ m}^{-1}$. We can assume that there is no plasma shielding and no defocusing of the laser beam (due to a plasma lens effect) in the plume during welding with a Nd:YAG laser.

C. Scattering in the plume

The laser-induced plasma is a semitransparent medium. We have given the absorption coefficient for different cases. In solving the radiative transfer equation, it is insufficient to consider only the absorption of the laser beam in the plume because we have also observed that small particles are present in the plume. Consequently, the laser beam may also be scattered inside the plasma. In order to measure the size of the particles present in the plume, we placed a thin glass plate in the laser beam path, on the lower face of which the metallic vapors are deposited when the plasma plume is initiated. The plates were viewed under an electron microscope. The compositions of the deposits, mainly oxides (FeO 57.43%, Cr_2O_3 24.11%, MnO 7.14%, NiO 6.59%, and SiO_2 4.73%), are similar to those estimated in the density calculations. Figures 5 and 6 present photographs of the metallic deposit, magnified 800 and 50 000 times.

In the first picture, we see that the deposit is an accumulation of small particles, with larger particles approximately $1 \mu\text{m}$ in diameter. The second photograph gives a larger view of one of these large particles showing it as an agglom-

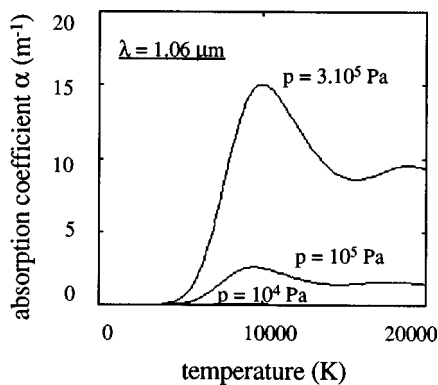


FIG. 4. Absorption coefficient vs temperature for different pressures.

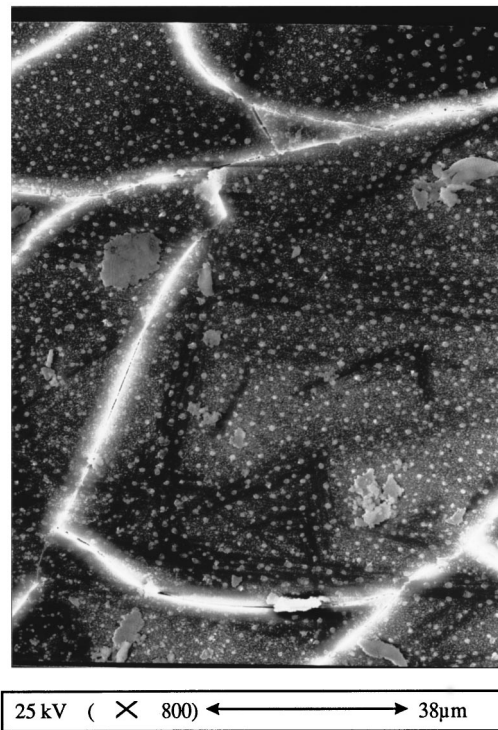


FIG. 5. Metallic deposit 800x magnification.

erate of very small particles, of around 50 nm. We conclude that the plasma plume is made of very small particles, which condense into larger droplets on the glass plate.

To simplify the calculations, the particles in our model are considered as spheres. The bidirectional scattering coefficients are calculated by applying Maxwell's equations for

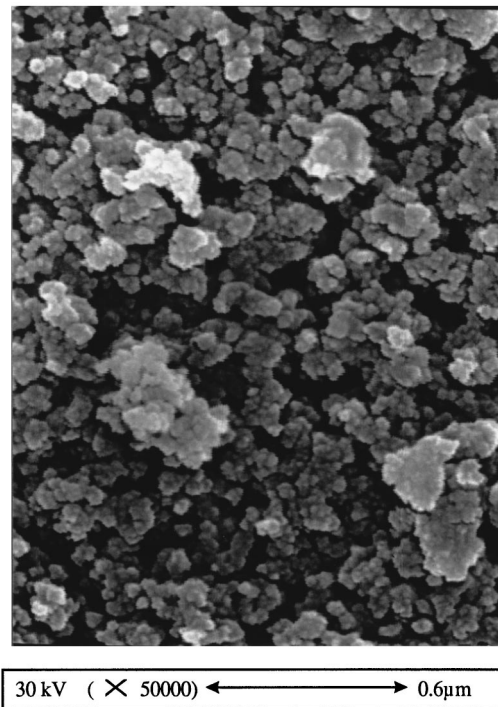


FIG. 6. Metallic deposit 50×10^3 x magnification.

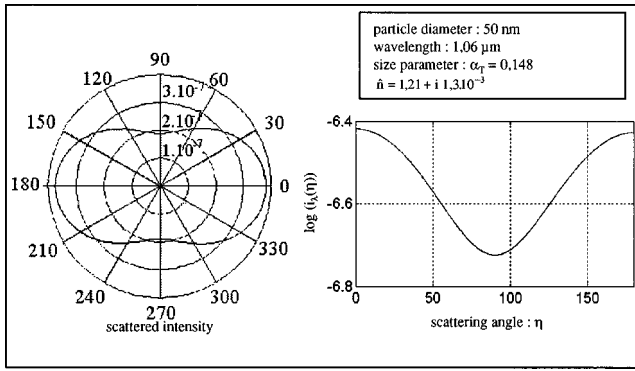


FIG. 7. Phase function for a small particle.

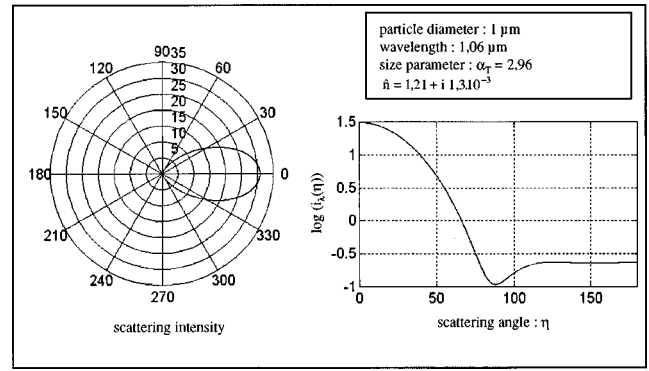


FIG. 8. Phase function for a large particle.

an electromagnetic wave interacting with a semitransparent particle. The different stages of the calculation are: (i) determination of coefficients a_n and b_n for a given particle, (ii) calculation of the scattering, absorbing, and extinction efficiencies, (iii) determination of the corresponding scattering geometry, and (iv) summation on a medium consisting of several particles.

Coefficients a_n and b_n have been calculated by Kerker¹⁴ using Riccati–Bessel functions (ψ_n and χ_n) such that:

$$a_n = \frac{\psi_n(\alpha_T)\psi'_n(\beta) - \hat{n}\psi_n(\beta)\psi'_n(\alpha_T)}{\zeta_n(\alpha_T)\psi'_n(\beta) - \hat{n}\psi_n(\beta)\zeta'_n(\alpha_T)}, \quad (10)$$

$$b_n = \frac{\hat{n}\psi_n(\alpha_T)\psi'_n(\beta) - \psi_n(\beta)\psi'_n(\alpha_T)}{\hat{n}\zeta_n(\alpha_T)\psi'_n(\beta) - \psi_n(\beta)\zeta'_n(\alpha_T)}, \quad (11)$$

where α_T is the size parameter, which depends on the radius of the particle and on the wavelength of the radiation,

$$\alpha_T = \frac{2\pi r}{\lambda} \quad (12)$$

and

$$\beta = \alpha_T \hat{n}. \quad (13)$$

The three efficiencies are $Q_{s,\lambda}$, $Q_{a,\lambda}$, and $Q_{e,\lambda}$:

$$Q_{s,\lambda} = \frac{2}{\alpha^2} \sum_{n=1}^{\infty} (2n+1) \{|a_n|^2 + |b_n|^2\}, \quad (14)$$

$$Q_{e,\lambda} = \frac{2}{\alpha^2} \sum_{n=1}^{\infty} (2n+1) \{\text{Re}(a_n + b_n)\}, \quad (15)$$

$$Q_{a,\lambda} = Q_{e,\lambda} - Q_{s,\lambda}. \quad (16)$$

The scattering, absorbing, and extinction coefficients $\sigma_{\lambda,s}$, $\sigma_{\lambda,a}$, and $\sigma_{\lambda,e}$ can be found readily from the efficiencies and with the volume fraction of the medium f_v , which is the ratio of the particle volume to the plume volume. We have:

$$\sigma_{\lambda} = \frac{3f_v}{4r} Q_{\lambda}. \quad (17)$$

Figures 7 and 8 present the phase function for two size parameters: 0.148 and 2.96, which correspond to particle radii of 25 nm and 0.5 μm . Each figure gives a polar plot of the diffused irradiance versus the scattering angle, plus a graph

of the logarithms of parallel and perpendicular polarized intensity versus the scattering angle. It can be seen in Fig. 7 that the phase function verifies the Rayleigh law. The incoming radiation is isotropically diffused. For the bigger particles (Fig. 8), the forward-scattered irradiance is more than 100 times greater than the backscattered. This directional asymmetry becomes more pronounced as the size parameter increases.

III. RADIATIVE TRANSFER

A. Radiative transfer in a semitransparent medium

A semitransparent medium participates in the radiative transfer by absorption, emission, and scattering. The radiative energy balance allows us to write the radiative transfer equation

$$\begin{aligned} \frac{\partial L_{\lambda}(s, \Omega)}{\partial s} + [\sigma_{\lambda,a} + \sigma_{\lambda,s}(\Omega)]L_{\lambda}(s, \Omega) \\ = \sigma_{\lambda,a}L_{\lambda}^0(T) + \frac{1}{4\pi} \int_{\Omega=4\pi} \sigma_{\lambda,s}(\Omega', \Omega) \\ \times \phi_{\lambda}(\Omega', \Omega)L_{\lambda}(s, \Omega')d\Omega', \end{aligned} \quad (18)$$

where L_{λ}^0 is the monochromatic intensity, L_{λ}^0 the blackbody intensity, Ω the direction of radiative propagation, and ϕ_{λ} the phase function.

The net radiative energy can be expressed from the radiative flux vector $q_{s,\lambda}$,

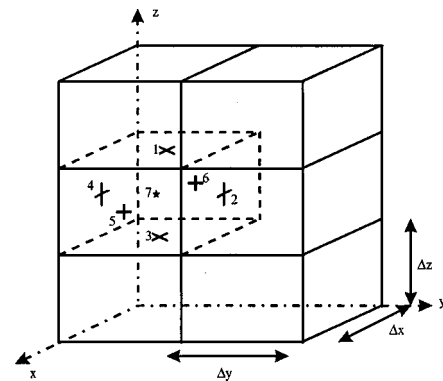


FIG. 9. Grid description.

$$q_{s,\lambda} = - \int_{\Omega=4\pi} \frac{\partial L_{\lambda}(s, \Omega)}{\partial s} d\Omega. \tag{19}$$

If we integrate relation (18) over all directions of space, considering the phase function normalized, we can rewrite the radiative transfer equation as follows:

$$q_{s,\lambda} = \int_{\Omega=4\pi} \sigma_{\lambda,a} L_{\lambda}(s, \Omega) d\Omega - \int_{\Omega=4\pi} \sigma_{\lambda,a} L_{\lambda}^0(T) d\Omega. \tag{20}$$

We assume that the intensity is isotropic in reflection and emission at the field boundaries. Applying Kirchhoff's law, we can write

$$L_{\lambda}(s_0, \Omega) = \varepsilon_{\lambda}(s_0) L_{\lambda}^0(T) + \frac{[1 - \varepsilon_{\lambda}(s_0)]}{\pi} \times \int_{\Omega'=2\pi} L_{\lambda}(s_0, \Omega') \cos(\theta) d\Omega'. \tag{21}$$

$$\begin{aligned} &\mu_m A [L_{5,\lambda}(x, y, z, m) - L_{6,\lambda}(x, y, z, m)] + \xi_m B [L_{2,\lambda}(x, y, z, m) - L_{4,\lambda}(x, y, z, m)] + \eta_m C [L_{1,\lambda}(x, y, z, m) - L_{3,\lambda}(x, y, z, m)] \\ &+ \vartheta(\sigma_{\lambda,a} + \sigma_{\lambda,s}) L_{7,\lambda}(x, y, z, m) = \vartheta \sigma_{\lambda,a} L^0(T) + \vartheta \frac{\sigma_{\lambda,s}}{4\pi} \sum_{m'} \phi_{\lambda}(m', m) W_{m'} L_{7,\lambda}(x, y, z, m'), \end{aligned} \tag{22}$$

with

$$A = \Delta y \Delta z, \quad B = \Delta x \Delta z, \quad C = \Delta x \Delta y, \quad \vartheta = \Delta x \Delta y \Delta z.$$

At the boundaries of the medium, Eq. (21) can be discretized. For example, if we consider the top face (index $i = 1$) we have

$$\begin{aligned} L_{1,\lambda}(x, y, z, m) &= \varepsilon_1 L^0(T_1) \\ &+ \frac{(1 - \varepsilon_1)}{\pi} \sum_{m'} L_{1,\lambda}(x, y, z, m') |\eta_{m'}| W_{m'}, \end{aligned} \tag{23}$$

with $\eta_{m'} > 0$. To calculate the intensity field, we start the processing at each corner of the mesh. We need relations between the intensities on two opposite sides of the cell. These relations can be simple average values of the intensities on each facing side of a cell:

$$L_{7,\lambda}^m = \frac{L_{1,\lambda}^m + L_{3,\lambda}^m}{2} = \frac{L_{2,\lambda}^m + L_{4,\lambda}^m}{2} = \frac{L_{5,\lambda}^m + L_{6,\lambda}^m}{2}. \tag{24}$$

The intensity field in the medium, obtained with relations (22), (23), and (24), contains anomalous computational effects due to the discretization of the angular variable in the radiative transfer equation. These are called ‘‘ray effects.’’

To eliminate these effects, we used relations including the optical properties of the medium (absorption and scattering). We developed these relations on the basis of the theory of Lathrop and Carlson,¹⁸ who studied the ray effect disturbance for a bidimensional geometry. We have

$$L_{7,\lambda}^m = f_z L_{1,\lambda}^m + (1 - f_z) L_{3,\lambda}^m, \tag{25}$$

B. The discrete ordinate method

There are several ways of solving the radiative transfer equation (Monte Carlo, zone, multiflux, and other methods). The discrete ordinate method was first developed by Chandrasekhar,¹⁵ then by Truelove and Hyde¹⁶ for the non-scattering medium, and Fiveland¹⁷ for the absorbing and scattering medium. To apply this method, we transform the radiative transfer equation (18), choosing a finite number of radiative directions of propagation, and describe the plasma plume using a Cartesian mesh.

The discrete directions of propagation are defined by their cosine directors (μ , ξ , and η). In our calculations, we used the S_4 quadrature, which defined 24 directions. The plasma plume grid is shown in Fig. 9. Each face of the cell is marked by an index (1–6), and index 7 stands for the center of the volume. Using this notation, we model the radiative transfer equation in the Ω_m direction as follows:

in which

$$f_z = \max(f'_z, \frac{1}{2}) \quad \text{with} \quad f'_z = 1 \frac{\alpha \beta}{\gamma[\alpha \beta + 2(\alpha + \beta)]}, \tag{26}$$

where

$$\alpha = \frac{\sigma \Delta x}{\mu}, \quad \beta = \frac{\sigma \Delta y}{\xi}, \quad \gamma = \frac{\sigma \Delta z}{\eta}, \quad \sigma = \sigma_{\lambda,a} + \sigma_{\lambda,s}. \tag{27}$$

The coefficients f_x and f_y are obtained like f_z , by changing the values of α , β , and γ . With relations (22), (25), and (26), the intensity at the center of the cell can be expressed as

$$L_7^m = \frac{\frac{|\mu_m| A L_6^m}{f_x} + \frac{|\xi_m| B L_4^m}{f_y} + \frac{|\eta_m| C L_3^m}{f_z} + \vartheta(S1 + S2)}{\frac{|\mu_m| A}{f_x} + \frac{|\xi_m| B}{f_y} + \frac{|\eta_m| C}{f_z} + \vartheta(\sigma_{\lambda,a} + \sigma_{\lambda,s})}, \tag{28}$$

where $A = \Delta y \Delta z$, $B = \Delta x \Delta z$, $C = \Delta x \Delta y$, $\vartheta = \Delta x \Delta y \Delta z$, and

$$S1 = \sigma_{\lambda,a} L^0(T), \quad S2 = \frac{\sigma_{\lambda,s}}{4\pi} \sum_{m'} \phi_{\lambda}(m', m) W_{m'} L_{7,\lambda}^{m'}.$$

C. Numerical results

The radiative transfer computation program was written in FORTRAN. We consider a cubic plasma plume 5 mm long. The mesh dimension is 35 elements in x and y , and 15 in z . The grid size is limited by the computer capacity. The boundary conditions of the model are: (i) The gas temperature is high enough and the emissivity value is set to $\epsilon = 0.9$, and (ii) The flux is zero at the boundary, i.e., we assume that

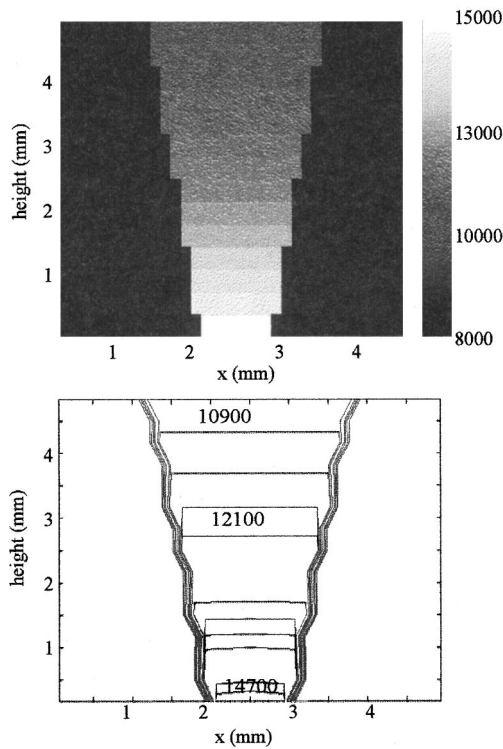


FIG. 10. Temperature variation without scattering.

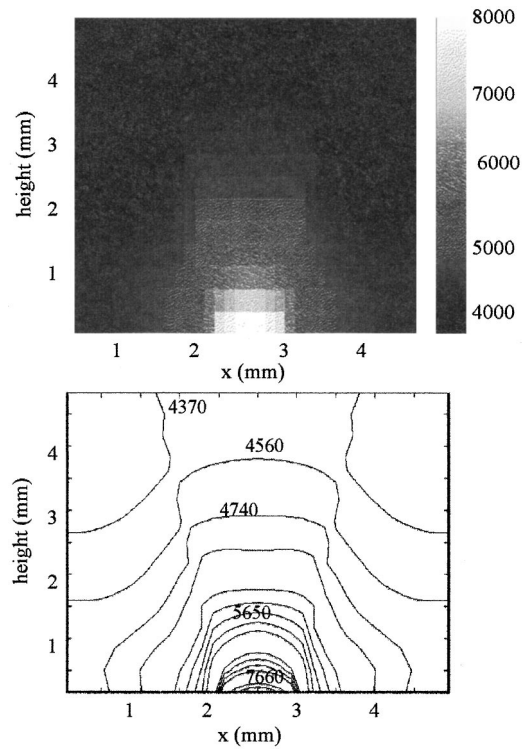


FIG. 11. Temperature variation with scattering due to small particles.

we have the ideal case of no heat transfer out of the medium (neglecting conduction and convection). The laser beam energy is a Gaussian distribution and the focal length of the laser is 120 mm. The laser power is set to 1000 W. Figure 10 presents the temperature variation inside the plume for a pure absorbing medium with no scattering of the laser beam.

The computed temperatures are rather high for a Nd:YAG laser interaction. Nevertheless, Mazumder *et al.*¹⁹ have shown that the irradiation of a gas such as argon by a 2.4 kW CO₂ laser may induce a plasma with temperatures as high as 15 000 K. Our case is similar: the isotherms on Fig. 10 indicate that the laser beam is still focused in the plume, the hottest part being in the focused cone.

Figure 11 shows the effect of small-particle scattering on the laser-plasma plume interaction. The particle diameter is 50 nm, the volume ratio is $f_v=5\%$. The effect of scattering in the laser welding process can be clearly seen here. For small values of the size parameter α_T , the laser light is scattered isotropically. A large portion of the incoming light is scattered in the backward direction. We observe that the warmer part of the plasma plume is widened at the bottom.

In Fig. 12, we show the case for bigger spheres (diameter 1 μm) with the same volume ratio as before (5%). For large-particle diameters, the phase function is oriented in the forward direction. The laser beam is not scattered greatly inside the plume. The hottest part of the plasma is in the path of the laser beam.

Laser-induced plasma temperature measurements were performed previously^{10,11} with a spectroscopic device during Nd:YAG welding, showing that the temperature in the plume ranges from 3500 to 7000 K, depending on the laser power and the processing parameters. So, we can consider that the

most realistic modeling results are for small particle diameters. Moreover, electron microscopy observations indicate that the plume contains basically small particles. This scattering phenomenon may explain the nail-head shape of the welding seam. In this case we can see that the laser beam is widened at the bottom of the plume. We performed other

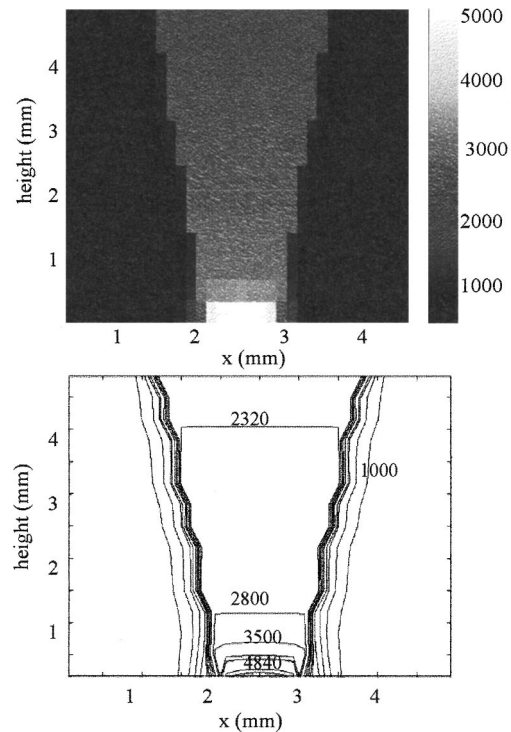


FIG. 12. Temperature variation with scattering due to large particles.

calculations to see what effect the volume ratio f_v would have on the results. As f_v decreases, the plume temperature increases.

IV. CONCLUSION

This study discusses certain aspects of beam scattering in laser welding. We first presented several models for calculating the plasma plume properties, such as the densities and the complex optical index. Then, we used Mie's theory to compute the scattering parameters of the plume. The final point of this study was the calculation of the radiative transfer in the plasma plume. The results obtained with the discrete ordinate method are in good agreement with the spectroscopic measurements for small particle diameters. We have given an explanation for the nail-head shape of the weld seam observed in Nd:YAG welding, in which the beam widening cannot be explained as defocusing due to a change of the refraction index inside the plume. This model can be improved by introducing more directions of propagation, and by considering the heat loss due to the conduction and convection around the plume. Nevertheless, this study gives details that might interest those working on weld seam geometry calculations in laser welding. The estimated laser beam flux at the bottom of the plume can be used as a boundary condition for numerical descriptions of the weld seam.

- ¹W. M. Steen, J. Dowden, M. Davis, and P. Kapadia, *J. Phys. D* **21**, 1255 (1988).
- ²B. R. Finke, P. Kapadia, and J. Dowden, *J. Phys. D* **23**, 643 (1990).
- ³J. Dowden and P. Kapadia, *J. Phys. D* **28**, 2252 (1995).
- ⁴C. Tix and G. Simon, *Phys. Rev. E* **50**, 453 (1994).
- ⁵M. Beck, P. Berger, and H. Hügel, *J. Phys. D* **28**, 2430 (1995).
- ⁶A. Matsunawa and T. Ohnawa, *Trans. JWRI* **20**, 9 (1991).
- ⁷A. Poueyo-Verwaerde, R. Fabbro, and G. Deshors, *J. Appl. Phys.* **78**, 2981 (1995).
- ⁸E. Dumord, thesis, University of Bourgogne (1996).
- ⁹H. Gouveia, I. Richardson, P. Kapadia, J. Dowden, and R. Ducharme, *Proceedings of the International Conference on Lasers and Electro-Optics, ICALEO'94*, Orlando, FL, Oct. 24–28, 1994, Laser Inst. America, Vol. 79, pp. 480–489 (1995).
- ¹⁰D. Lacroix, G. Jeandel, and C. Boudot, *Proc. SPIE* **2789**, 221 (1996).
- ¹¹D. Lacroix, G. Jeandel, and C. Boudot, *J. Appl. Phys.* **81**, 6599 (1997).
- ¹²B. S. Tannenbaum, *Plasma Physics* (McGraw-Hill, New York, 1973).
- ¹³M. Mitchener and C. H. Kruger, *Partially Ionized Gases* (Wiley, New York, 1973).
- ¹⁴M. Kerker, *The Scattering of Light and Other Electromagnetic Radiation* (Academic, New York, 1969).
- ¹⁵S. Chandrasekhar, *Radiative Transfer* (Dover, New York, 1960).
- ¹⁶J. S. Truelove and D. J. Hyde, Oxfordshire, A.E.R.E. Harwell, R-8502, p. 39 (1977).
- ¹⁷W. A. Fiveland, A.S.M.E. paper, 82-HT-20, pp. 1–8 (1982).
- ¹⁸K. D. Lathrop and B. Carlson, *Transport Theory—The Method in Reactor Physics*, edited by H. Greenspan, C. N. Kelber, and D. Okrent (Gordon and Breach, New York, 1968).
- ¹⁹J. Mazumder, T. J. Rockstroh, and H. Krier, *J. Appl. Phys.* **62**, 4712 (1987).